Supporting Information for

PoroFluidics: Deterministic fluid control in porous microfluidics

Zhongzheng Wang[1,+], Louis Jun Ye Ong[1-3,+], Yixiang Gan[5,6], Jean-Michel Periera[7], Jun Zhang[8], Surasak Kasetsirikul[1-2], Yi-Chin Toh[1-4,*], and Emilie Sauret[1,*]

[1]School of Mechanical, Medical and Process Engineering, Faculty of Engineering, Queensland University of Technology, QLD 4001, Australia
[2]Centre for Biomedical Technologies, Queensland University of Technology, QLD 4059, Australia
[3]Max Planck Queensland Centre, Queensland University of Technology, QLD 4059, Australia
[4]Centre for Microbiome Research, Queensland University of Technology, QLD 4102, Australia
[5]School of Civil Engineering, The University of Sydney, NSW 2006, Australia
[6]Sydney Nano, The University of Sydney, NSW 2006, Australia
[7]Navier, Ecole des Ponts, Univ Gustave Eiffel, CNRS, Marne-la-Vallée, France
[8]Queensland Micro and Nanotechnology Centre, Griffith University, Brisbane, QLD 4111, Australia
[+]These authors contributed equally to this work

Corresponding to: emilie.sauret@qut.edu.au (E. Sauret); yichin.toh@qut.edu.au (Y.C. Toh).

This PDF file includes:

Other supporting materials for this manuscript include the following:

Supporting Information Text

Pore-resolved interface tracking algorithm. The numerical algorithm adopted in this work is the recently developed pore-resolved interface tracking algorithm [1]. The algorithm allows the explicit determination of critical capillary pressure associated with different pore-scale invasion mechanisms based on interfacial tension, wettability, and pore geometry. Several menisci movement mechanisms are shown in Fig. S2(A-C). During simulation time, the meniscus with the smallest capillary resistance advances at each computation step, until the invading fluid percolates the porous media, i.e., when it reaches the outlet. In our previous study, we conducted multiphase simulations in a single junction micromodel with different channel widths, wetting conditions, and boundary conditions. It was shown that the experimentally observed pore-scale mechanisms can be captured, such as meniscus pinning due to the presence of sharp corners, cooperative pore-filling events, as well as corner trapping [1].

Fig. S2(D) shows a magnified region during a multiphase simulation in poroFluidics under the hydrophobic condition. The dry and wetted nodes are denoted as grey and blue dots, respectively. To incorporate the contact angle variations, we assign each pillar with contact angles obtained from a normal distribution according to the given mean and standard deviation [Fig. S2(E)]. We note a recent investigation on multiphase flow in mixed-wet porous media found that the fluid-fluid interface shape can deviate from a circle, forming an S-shaped saddle, when the contact angle heterogeneity is large, e.g., cylindrical pillars with contact angles being either $\theta = 60^\circ$ or $\theta = 120^\circ$ [2]. In our study, the solid wettability is relatively uniform and the assumption in the numerical algorithm that the interface remains in the shape of an arc is found to be valid.

Although the porous media in the current work are composed of circular posts, we want to emphasize the interface tracking algorithm's capability for simulating multiphase flow in porous media with more geometrically complex structures. Fig. S2(F) shows the snapshots from a simulation for an immiscible fluid-fluid displacement process in a representation of Berea sandstone [3]. Fig. S2(G) shows the simulation results from the multi-component lattice Boltzmann method [4]. It can be seen that the spatial and temporal invasions are consistent between these results. However, the computation time is less than 1 minute on a standard desktop computer for the interface tracking algorithm, whereas being more than 10 hours for the lattice Boltzmann method. This highlights the efficiency and versatility of the algorithm that can be applied to design poroFluidics with more complex geometries. A detailed description of the algorithm can be found in a previous study [1]. The code is available on Github [5].

Evaluation of flow path. In this work, the quantitative analyses of the critical capillary pressures based on pore-scale mechanisms are performed based on uniform sizes of pillars. This implies that, take the poroFluidic in Fig. S3 (A) as an example, the critical capillary pressures for the menisci between pillars of different sizes (red and blue circles) are in between those menisci that are either in contact with large posts only or smaller posts only. This corresponds to a buffer zone (regions between black-solid lines and black-dashed lines) that could be potentially invaded during the flow.

Fig. S3 shows the design schematic, simulation, and experiment for the hydrophobic (top row) and hydrophilic (bottom row) solid structures. Thus, the desired flow paths (or the invasion morphology) are regions enclosed by black-solid lines, whereas the regions outside the black-dashed lines should not be filled. It is clearly demonstrated that both the numerical simulations and experiments under different wetting conditions confirm the validity of the framework for poroFluidic design. We note that it is possible to explicitly determine the critical capillary pressure between posts of different sizes [6,7]. However, as one may expect more strict control of interface locations is associated with more demanding surface uniformity and solid manufacture resolution.

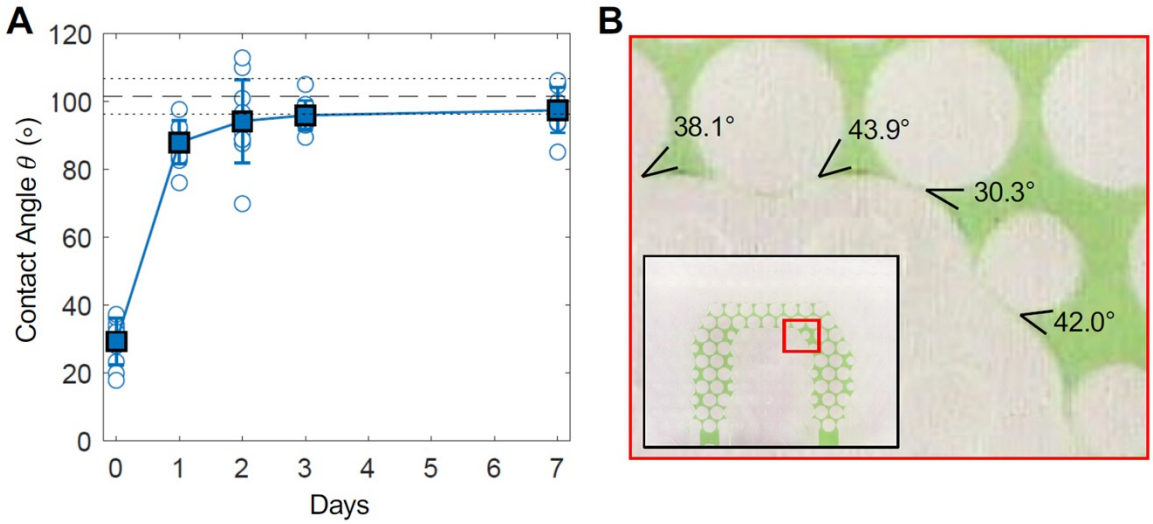

Fig. S1. Characterization of contact angles. (A) Measured contact angles by sessile drop method using ImageJ as a function of elapsed time after plasma treatment. The measurements were conducted within 30 minutes after treatment, and daily for up to seven days. Filled squares, error bars, and circles represent the mean, standard deviations, and raw measurements, respectively. The black-dashed line and black-dotted lines respectively represent the mean and standard deviation of contact angles measured from reference PDMS surfaces without any treatment. (B) A representative photo of a magnified region during a fluid injection experiment for the hydrophilic solid structure. The water (green) contact angles are indicated. The inset shows the zoomed-out region.

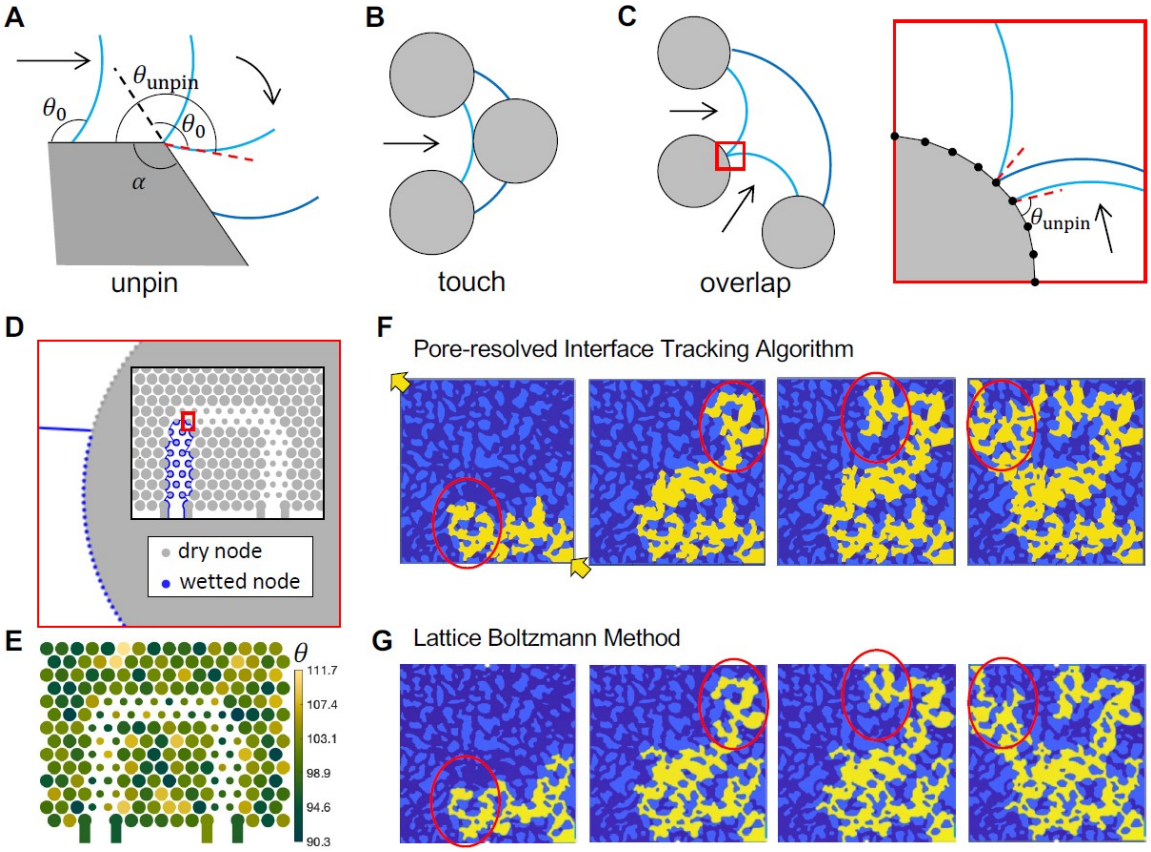

Fig. S2. Pore-resolved interface tracking algorithm. (A) A schematic of the unpin event that includes the successive motion of a fluid-fluid interface along the surface with a sharp corner. (B) An example of a touch event during which the meniscus touches a grain, splitting into two menisci. (C) The overlap event is when the two menisci merge into one meniscus. The black dots in the magnified image denote the computation nodes. The direction of menisci motion is indicated by black arrows. Light blue and dark blue curves, respectively, indicate the interface location before and after the corresponding event. (D) A magnified region during a simulation of fluid flow in poroFluidics. The dry and wetted nodes are in grey and blue colors, respectively. The post radii are generated from a normal distribution with standard deviation $\delta_r = 5.67\ \mu$m and average diameters $500\ \mu$m and $887\ \mu$m for small and large posts, respectively. (E) The heterogeneity in wettability from the simulated solid structure. Color variations represent different contact angles generated from a normal distribution with a mean of $\theta = 100.4^\circ$ and a standard deviation of $\delta_\theta = 4.28^\circ$. (F) Snapshots from a simulation for an immiscible fluid-fluid displacement process in a representation of Berea sandstone using the interface tracking algorithm. Yellow, light blue, and dark blue respectively represent injected fluid, solid, and defending fluid. The invading fluid (yellow) is injected from the bottom-right corner. The simulation stops when the yellow fluid reaches the outlet located at the top-left corner. (G) Corresponding simulation using the multi-component lattice Boltzmann method. Red circles in (F) and (G) highlight the general consistency in the invasion sequence between (F) and (G).

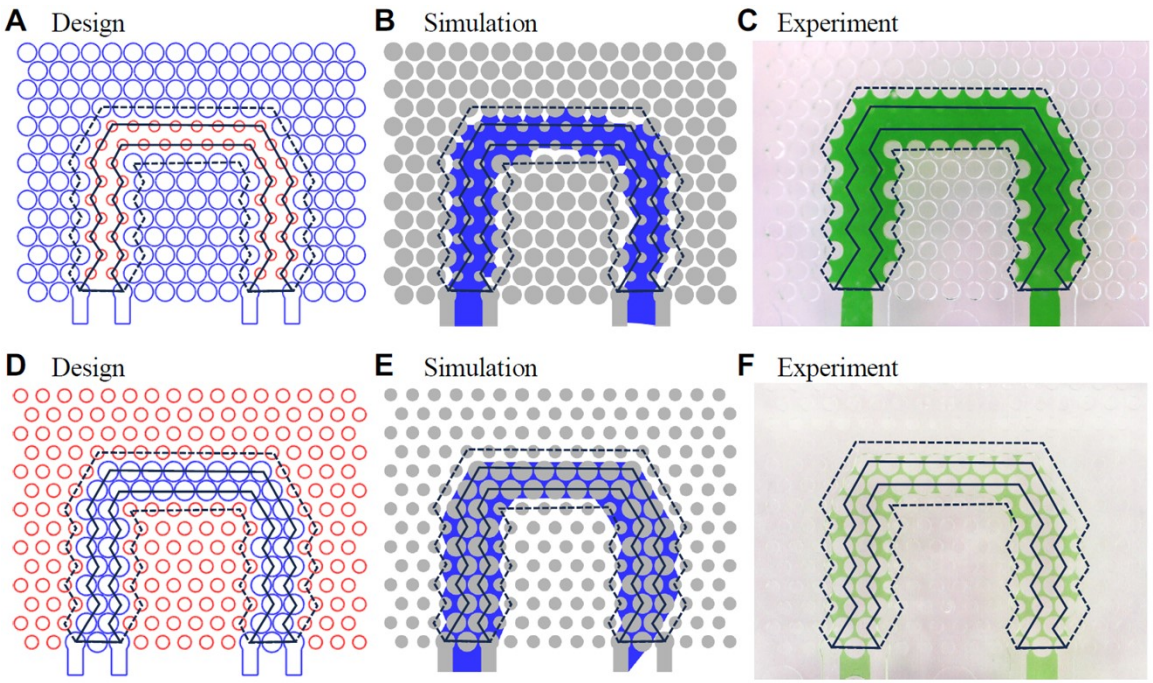

Fig. S3. Evaluation of fluid path. The schematic of the geometry design, simulation result, and experimental result for the hydrophobic solid structure $\theta = 100.4^\circ$) are shown in (A), (B), and (C), respectively. Results for the hydrophilic structure $\theta = 37.4^\circ$) are shown in (D), (E), and (F). According to mechanistic analyses, the regions to be filled are enclosed by solid black lines. The regions outside the black-dashed lines should not be filled.

Movie S1 (separate file). Water invasion sequence – simulation – hydrophobic

Movie S2 (separate file). Water invasion sequence – experiment – hydrophobic

Movie S3 (separate file). Water invasion sequence – simulation – hydrophilic

Movie S4 (separate file). Water invasion sequence – experiment – hydrophilic

Movie S5 (separate file). Branch-first invasion – simulation

Movie S6 (separate file). Branch-first invasion – experiment

Movie S7 (separate file). Stem-first invasion – simulation

Movie S8 (separate file). Stem-first invasion – experiment

Movie S9 (separate file). Gravity-regulated invasion – simulation – no gravity

Movie S10 (separate file). Gravity-regulated invasion – simulation – with gravity

Movie S11 (separate file). Wettability-regulated invasion – simulation – hydrophilic

Movie S12 (separate file). Wettability-regulated invasion – simulation – hydrophobic

SI References

1. Wang, Z. et al. A pore-resolved interface tracking algorithm for simulating multiphase flow in arbitrarily structured porous media. Adv. Water Resour. 162, 104152 (2022)
2. Irannezhad, A., Primkulov, B. K., Juanes, R. & Zhao, B. Fluid-fluid displacement in mixed-wet porous media. Phys. Rev. Fluids 8, L012301 (2023)
3. Guo, F. & Aryana, S. A. An experimental investigation of flow regimes in imbibition and drainage using a microfluidic platform. Energies 12 (2019).
4. Wang, Z., Pereira, J.-M. & Gan, Y. Effect of wetting transition during multiphase displacement in porous media. Langmuir 36, 2449–2458 (2020).
5. Wang, Z. ITA multiphase. https://github.com/Spoonacular/ITA_multiphase (2023).
6. Primkulov, B. K. et al. Quasistatic fluid-fluid displacement in porous media: Invasion-percolation through a wetting transition. Phys. Rev. Fluids 3, 104001 (2018).
7. Hu, R., Lan, T., Wei, G.-J. & Chen, Y.-F. Phase diagram of quasi-static immiscible displacement in disordered porous media. J. Fluid Mech. 875, 448–475 (2019).